PERGAMON

Vacuum 63 (2001) 337–344

VACUUM
SURFACE ENGINEERING, SURFACE INSTRUMENTATION & VACUUM TECHNOLOGY

www.elsevier.nl/locate/vacuum

Interface modeling in Cr/Fe/Cr sandwiches studied by CEMS

M. Kubik[a], T. Ślęzak[a], M. Przybylski[a], W. Karaś[a], J. Korecki[a,b,*]

[a]*Department of Solid State Physics, Faculty of Physics and Nuclear Techniques, University of Mining and Metallurgy, Al. Mickiewicza 30, 30-059 Kraków, Poland*

[b]*Institute of Catalysis and Surface Chemistry, Polish Academy of Sciences, ul. Niezapominajek 8, 30-239 Kraków, Poland*

Abstract

Conversion electron Mössbauer spectroscopy (CEMS) was applied to model the buried interfaces in epitaxial 1–14 monolayer (ML) Fe(0 0 1) films sandwiched between Cr(0 0 1) layers. The local arrangement of Fe and Cr was derived by analysis of the experimental hyperfine field distributions determined from 80 K CEMS spectra. A discontinuity in magnetic properties for the 6 ML Fe film suggests that a modification of the magnetic structure occurs at this thickness. The ^{57}Fe probe layer analysis showed that Cr/Fe and Fe/Cr interfaces are non-equivalent. The lower interface showed up to be smoother than the upper one. The Fe concentration profile obtained form the CEMS analysis displayed a considerable interface Fe–Cr alloying for films deposited at the room temperature.

PACS: 75.70.Ak; 76.80. + y

Keywords: CEMS; Fe; Cr; Ultra thin epitaxial films; Interface structure; Alloying

1. Introduction

The last decade brought a tremendous interest in magnetic systems of nanometer thickness [1], mainly due to their application in recording technique. Particularly, the indirect coupling phenomenon that leads the ferro- or antiferromagnetic arrangements of the sub-layer spins is of special attention and importance because the last is accompanied by the giant magnetoresistance (GMR) observed for the first time in the Fe/Cr/Fe system [2]. The indirect exchange coupling between ferromagnetic layers separated with a nonmagnetic spacer depends strongly on the atomic structure of the interfaces. It has been suggested that roughness and atomic interface intermixing between Fe and Cr is responsible for this effect [3]. Interface roughness suppresses the short-range (with the period of 2 Cr monolayers) coupling oscillations, leaving the long-range ones (with the period of 12 Cr monolayers). Additionally, for the Fe/Cr systems, the intrinsic and intricate antiferomagnetism of chromium [4], strongly modified in layered structures [5], is involved in the coupling. The model studies using single crystalline whisker substrates [6] are of a great importance for understanding the basic phenomena but often they do not relate directly to other systems, in which the resulting structure depends crucially on many

* Corresponding author. Faculty of Physics and Nuclear Techniques, University of Mining and Metallurgy, Al. Mickiewicza 30, 30-059 Krakow, Poland. Fax: + 48-12-643-1247.

E-mail address: korecki@uci.agh.edu.pl (J. Korecki).

0042-207X/01/$ - see front matter
PII: S0042-207X(01)00210-X

technological parameters. That is why we have undertaken detailed studies of Fe/Cr multilayers grown on the MgO(0 0 1) substrates, aimed to find the correlation between magnetic and structural properties. Here we report on the conversion electron Mössbauer spectroscopy (CEMS) experiments for single Fe films sandwiched between Cr layers. CEMS offers a unique possibility to analyze both, the structural and the magnetic properties of buried interfaces at atomic scale. Moreover, the isotopic sensitivity of the method allows depth profiling of iron films using a ^{57}Fe probe layer embedded during the growth in a film consisting otherwise of ^{56}Fe. The probe layer concept is here especially useful for verifying an asymmetry suggested for the Fe/Cr and Cr/Fe interfaces [7]. The atomic model of the single film interfaces obtained from the present analysis sets a basis for further studies of the coupling phenomena in the Fe/Cr multilayer systems.

2. Sample preparation and characterization

The sample preparation and the characterization was performed in situ, using a multi-chamber UHV system [8] with the base pressure 1×10^{-10} mbar. The system is equipped with a load-lock facility, a universal sample mounting and transfer system, standard surface characterization methods (a 4-grid electron optics for LEED and AES), a MBE system for deposition of several metals including ^{56}Fe and ^{57}Fe isotopes and Cr and a CEMS spectrometer. All samples were deposited on MgO(0 0 1) substrates that were cleaved ex situ in pure N_2 atmosphere prior to the introduction into the UHV system, where they were annealed at 400°C for 1 h. Such treatment resulted in a clean surface showing only traces of carbon contamination and a perfect background-free 1×1 LEED pattern. The whole structure of the Cr/Fe/Cr sandwiches was deposited on the as cooled substrates kept at about 330 K. Fe and Cr were deposited from BeO crucibles heated from wrap-around tungsten coils. The crucible assemblies were embedded in a water-cooled shroud and the pressure during the deposition was maintained in the 10^{-10} mbar range. The film thickness was controlled during the deposition by quartz thickness monitors with the accuracy of about 0.2 ML. In situ Mössbauer measurements were performed using an efficient 80–500 K CEMS spectrometer based on channeltron detection [8], with a 150 mCi ^{57}Co(Rh) source. The spectrometer geometry settled a fixed angle of 45° between the direction of the γ ray propagation and the sample normal. The room temperature spectra could be measured also ex situ with a flow proportional He/CH_4 detector and with the γ ray propagation direction parallel to the sample normal. For all samples, a 20 nm Cr buffer layer was used, on which ^{57}Fe films of the thickness varying between 1 and 14 (0 0 1) atomic layers were deposited. Finally, the Fe films were capped with 5 nm Cr.

Fig. 1 shows typical LEED patterns for the Mg(0 0 1) substrate (Fig. 1a) and for the Cr buffer layer (Fig 1b). A low intensity background and sharp spots in the whole range of the electron energy for the MgO substrate contrast with the feature observed for the Cr surface. To our knowledge, the epitaxy of Cr on MgO(0 0 1) was not reported before in the literature. The lattice spacings 0.407 nm for Cr along [1 1 0] and 0.420 nm for MgO along [1 0 0] are well matched when the both lattices are rotated by 45°. Accordingly, our LEED patterns clearly demonstrate the epitaxial growth with the geometrical relations identical as in the case of Fe on MgO(0 0 1), i.e. Cr(0 0 1) [001] $\parallel$ MgO(0 0 1) [0 1 1]. With increasing electron energy, all spots vary between sharp and diffused shape periodically. This behavior is typical for irregular steps with randomly distributed step heights, widths or edge orientation [9]. By analogy with STM studies of iron buffer layers deposited in the same conditions [10] and basing on crystallographic and electronic Fe and Cr similarity, we suppose that monoatomic steps with randomly varying terrace width are responsible for the observed LEED patterns. For the electron energy 95 eV fulfilling the out-of-phase conditions for (01) spots (Fig. 1b), the spot width is a measure of the average terrace width. A crude estimation, based on the comparison with simulations for steps with a Gaussian distribution of the terrace width [9], gives us the edge atom fraction of the order of 20% and respectively, assuming square terraces, the linear terrace dimension of a few nanometers.

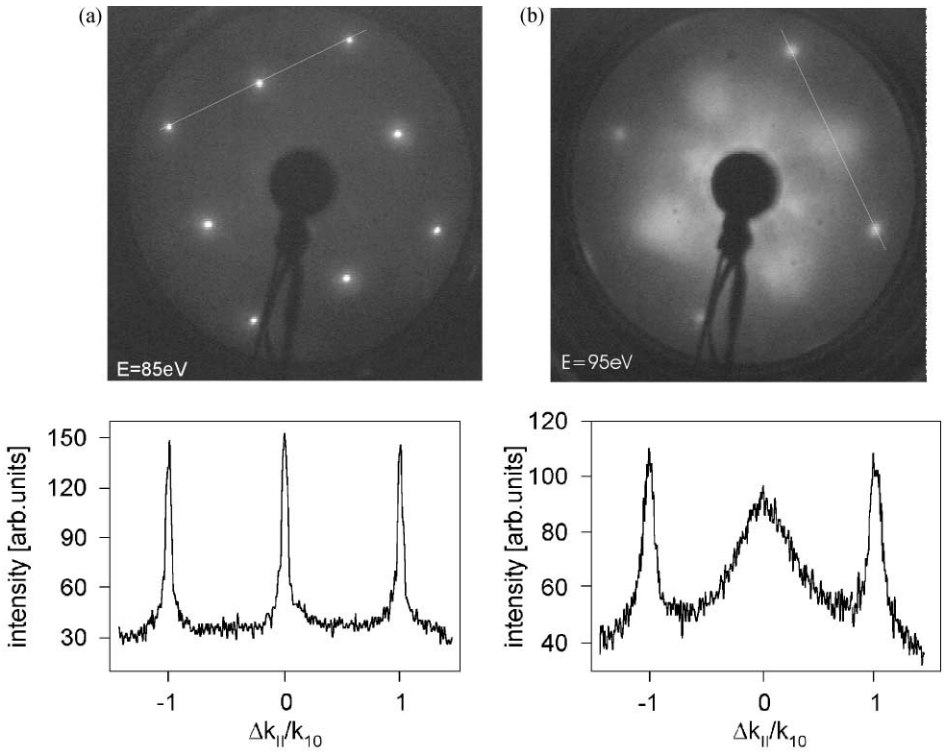

Fig. 1. LEED patterns and profiles for (a) the MgO(0 0 1) substrate at the electron energy 85 eV and (b) 20 nm Cr(0 0 1) buffer layer at 95 eV.

The LEED characteristic did not change substantially for the further deposited Fe layer and also for the Cr cap layer. From the qualitative LEED analysis it seems however that upon the Fe deposition the surface becomes smoother as evidenced by narrowing of the spots in the out-of-phase conditions and by the lower level of the diffused background intensity.

In the following text, the symbol N denoting a sample $Cr/Fe_N/Cr$ is the number of the monoatomic layers in the final sandwich structure: MgO(0 0 1)/20 nm Cr(0 0 1)/N ML ^{57}Fe(001)/5 nm Cr(0 0 1). The thickness is given assuming that 1 Fe (Cr) (0 0 1) ML corresponds to 0.143 nm (0.144 nm) as follows from the bulk lattice constants.

3. Results and discussion of Mössbauer analysis

The CEMS spectra measured for $Cr/Fe_N/Cr$ sandwiches at 300 and 80 K are summarized in Fig 2a and b, respectively. All presented room temperature spectra were measured with the proportional counter, whereas the 80 K spectra were taken using the in situ UHV CEMS spectrometer. For the thinnest Fe films ($N = 1,2$), pronounced temperature effects are seen. Obviously, the Curie temperature for these films is below (for $N = 1$) or near the room temperature (for $N = 2$). The temperature-induced effects for all other samples are only quantitative, observed as a several percent increase of the hyperfine magnetic fields. However, already by the visual inspection strong differentiation of the spectra is seen with increasing the Fe film thickness. Up to $N = 5$ the spectra are characterized by a broad distribution of the hyperfine magnetic field. Then, abruptly, at $N = 6$, distinct spectral components with relatively narrow lines appear. Increasing the film thickness further makes the spectra dominated by a sharp bulk like component accompanied by a broader one (with a smaller hyperfine splitting), with the intensity decreasing going to the thicker

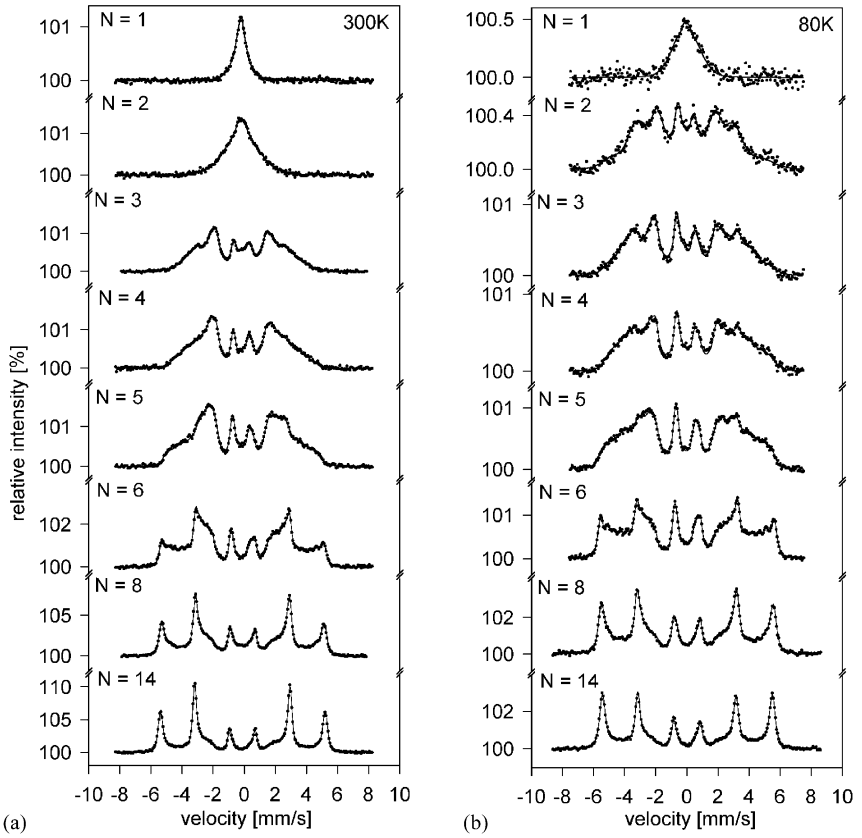

Fig. 2. The CEMS spectra for $Cr/Fe_N/Cr$ sandwiches measured at (a) 300 K and (b) 80 K. The solid lines are the numerical fits.

films. Obviously, in the simplest picture, the film interior contributes to the bulk-like component, whereas the broad distribution comes from interfacial Fe atoms. The broad distribution of the magnetic hyperfine fields may originate either from a structural and chemical disorder or from a specific magnetic structure. The magnetic hyperfine field B_{hf} at the ^{57}Fe nucleus is determined by the chemical coordination. It has been commonly assumed that for the Fe–Cr interface, the alloy analogy applies quite well [11,12] and the B_{hf} distribution reflects the distribution of the local atomic arrangements of the Fe and Cr atoms. In this model, the B_{hf} value at a given ^{57}Fe nucleus is lowered from the bulk Fe value by each Cr atom in the first and the second coordination shell:

$$B_{hf}(n_1, n_2) = B_{hf}(0,0) - c_1 n_1 - c_2 n_2, \quad (1)$$

where n_1 and n_2 are the numbers of the nearest and next nearest Cr neighbors of the given Fe atom and c_1 and c_2 are proportionality constants. The previously reported experimental c_1 and c_2 values differ only slightly for bulk [13] and for interfaces [12,14]. It has to be pointed-out that they depend on temperature and, especially for thinnest films, they should be derived from low temperature data. At the interfaces, in the ultra thin films, the number of allowed configurations is strongly limited by the planar geometry, however the interface roughness and alloying may smear out the chemical order characteristic for the sharp interface. The sudden change of the spectrum character observed for $N = 6$ could suggest that interface sharpening occurs for this film thickness. It is however not accompanied by any detectable changes in the corresponding LEED patterns. Therefore, we

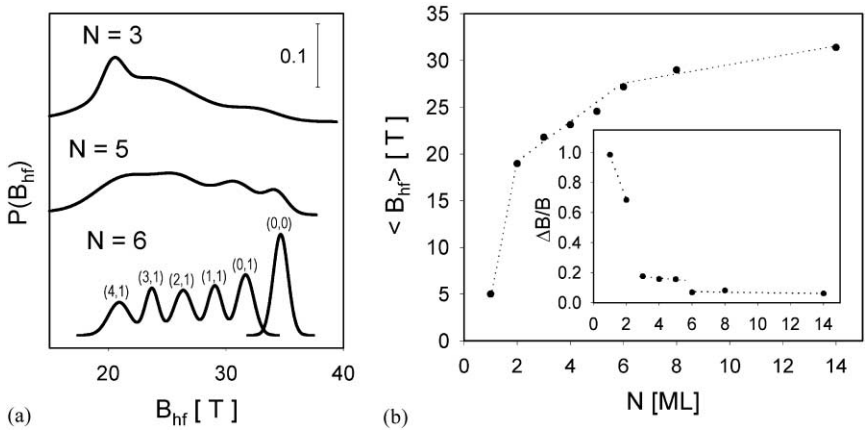

Fig. 3. The results of numerical fit for Cr/Fe_N/Cr sandwiches; (a) distribution of B_{hf} for selected samples. For $N = 6$, the distribution maxima are labeled with corresponding atomic configurations, according to the notation described in the text; (b) average $\langle B_{hf} \rangle$ values versus the film thickness N; (the inset in (b)) dependence of $\Delta B/B = [\langle B_{hf}(80\,K)\rangle - \langle B_{hf}(300\,K)\rangle]/\langle B_{hf}(80\,K)\rangle$ value on the film thickness.

incline toward the interpretation of a magnetic origin of the transition observed at $N = 6$. It can be due to a change of the magnetic structure (type of ordering, magnitude of the magnetic moments) in the Cr layers. Such phenomenon is highly probable in view of the sensitivity of the Cr magnetic structure to the size effects [5], structural modifications [15] or proximity of a magnetic layer [16].

The spectra were analyzed numerically by fitting a hyperfine field distribution (HFD) using the Voigt-based method of Rancourt and Ping [17]. The method describes the HFD by a sum of Gaussian components for the B_{hf}, isomer shift (IS) and quadrupole splitting (QS) distributions. Only a linear correlation between B_{hf} and IS or QS can be used in the numerical procedure, which might be an oversimplification, leading to a systematical error when a broad range of B_{hf} is analyzed. The number of Gaussian components was increased gradually from 1 such that a minimum number of fitting parameters were introduced. Once a statistically ideal fit was obtained, increasing the number of the component did not change the distribution or any of the essential fit parameters. The numerical fits are shown as the solid lines in Fig. 2 and their results are summarized in Fig. 3. Fig. 3a shows selected characteristic distribution of B_{hf}. It is clearly seen that the broad distributions for $N = 3$ and 5, with sharper maxima around 20 T, becomes peaked out at six well defined B_{hf} values for $N = 6$. A transition in magnetic properties is also apparent from the dependence of the average $\langle B_{hf} \rangle$ values on the film thickness N obtained from the fitted distributions (Fig. 3b). The $\langle B_{hf} \rangle$ dependence exhibits notable cusps. The first one, at $N = 2$, corresponds to the abrupt change of the configuration between 1 and 2 ML bcc films. In the (0 0 1) monolayer film, neglecting the deviation from the layer growth, all the Fe nearest neighbors (n.n.) are Cr atoms. For the 2 ML (0 0 1) film the number of the Fe n.n. increases by 4 and for the 3 ML (0 0 1) film all Fe n.n. atoms are already Fe atoms. The two first α-Fe-like coordination shells are restored only in the 5 ML (0 0 1) film. Filling the coordination shells by the Fe atoms explains the cusps in the $\langle B_{hf} \rangle$ versus N dependence but it cannot be responsible for the change in the character of the B_{hf} distribution. Even more intriguing is the influence of temperature on the average hyperfine magnetic field visualized by the inset in Fig. 3b as the dependence of the $\langle B_{hf} \rangle$ reduction between 80 and 300 K normalized to the 80 K value. The only plausible explanation of the discontinuities at $N = 3$ and 6 involves a change of the coupling between the Fe film and the Cr layers. This issue (it will be discussed further elsewhere [18])

emphasizes the importance of the interplay between the structural and magnetic properties, which must be considered in the interpretation of the Mössbauer spectra in terms of a structural model. Therefore, for the interface modeling, the 6 ML film has been chosen, for which the magnetic structure seems to be well established but still interfacial atoms contribute predominantly to the Mössbauer spectrum.

The character of the B_{hf} distribution for the 6 ML sample can be explained using Eq. (1). Six maxima in the B_{hf} distribution for $N = 6$ (Fig. 3a) are distinctly resolved. The high field maximum corresponds to the central part of the film, where the Fe atoms do not have Cr atoms as the n.n.'s and the next n.n.'s. Such configuration is denoted $(n_1, n_2) = (0,0)$, accordingly to the notation used in Eq. (1). The sharp interface would yield for the 6 ML film only two additional configurations: (4,1) for the surface interface layer and (0,1) for the subsurface one. The three additional maxima in the B_{hf} distribution for $N = 6$ in Fig. 3a, corresponding to the configurations (3,1), (2,1) and (1,1), are then due to a deviation from the perfect interface caused by steps or Fe–Cr interfacial alloying. From the maxima positions, the constants in Eq. (1) can be precisely determined as: $B_{hf}(0,0) = 34.5\,\mathrm{T}$, $c_1 = 2.99\,\mathrm{T}$ and $c_2 = 2.66\,\mathrm{T}$. The c_1 and c_2 values differ remarkably from those used in the previous interfaces studies [11,12,14]. The most striking difference is that our analysis gives $c_1 > c_2$, whereas in the previous studies the reverse relation was assumed basing on the data for dilute FeCr alloys [13]. Our methodology applies strictly to the ultra thin film interfaces, giving consistent results for a series of samples, it considers also the temperature effects, which may alter surface and subsurface B_{hf} components in a different way. Thus, we question using the bulk alloy parameters for the description of the interfacial hyperfine magnetic field with Eq. (1). Relation between hyperfine fields and atomic configurations in thin films may be considerably different than in the bulk.

Using the derived relation between the hyperfine magnetic field and the atomic configuration, the interface modeling was made by adjusting the concentration profile at the interfaces to reproduce the intensity of the peaks in the experimental B_{hf} distribution. A simple film model, assuming only monoatomic steps, was not able to reproduce the experimental B_{hf} distribution. Therefore, the interface zone was allowed to spread over few (2 or 3) atomic layers, where random two-dimensional Fe–Cr alloy was formed. Then the configuration probabilities were calculated accordingly to the binomial distribution and converted to the B_{hf} distribution using Eq. (1). Neither this procedure gave a satisfactory description. The best solution could

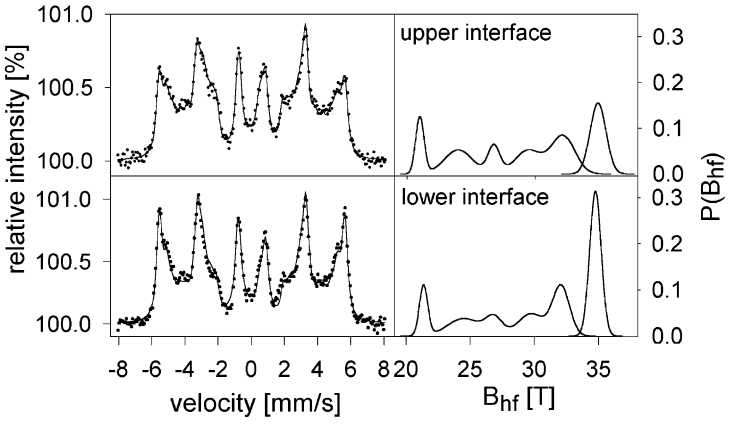

Fig. 4. ^{57}Fe probe layer analysis of the interfaces. The CEMS spectra of 6 ML Fe samples, in which at first 3 ML Fe^{57} (Fe^{56}) monolayers were deposited on the Cr buffer followed by 3 ML Fe^{56} (Fe^{57}) monolayers. The B_{hf} histograms resulting from numerical fits are shown with the spectra.

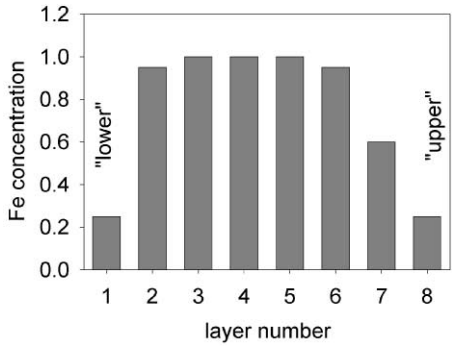

Fig. 5. The concentration profile of Fe in the film of the nominal thickness 6 ML.

be found assuming that both the interfaces, the "lower" one, formed when the Fe layer is deposited on the Cr buffer, and the "upper" one are non-equivalent. This assumption has been verified experimentally using the ^{57}Fe probe layer concept. Two special 6 ML Fe films were prepared, in which at first 3 ML ^{57}Fe (^{56}Fe) layers were deposited on the Cr buffer, and then followed by 3 ML ^{56}Fe (^{57}Fe). In the first samples the "lower", in the second one the "upper" interface were probed in the following CEMS measurements. The results of the probe layer CEMS measurements are show in Fig. 4. Indeed, the both interfaces are different as seen by the Mössbauer spectroscopy. The lower interface showed up to be smoother than the upper one. The CEMS spectrum of the upper interface is dominated by the broad interfacial components, whereas for the lower one, the contribution of the bulk-like component is not far from the value $\frac{1}{3}$ expected for the perfectly sharp and smooth boundary between Cr and Fe. The relative contribution of the spectral components cannot be taken directly as the measure of the composition because isotope intermixing can take place during the deposition. Nevertheless, the probe layer analysis clearly proved that the growths of Fe on Cr and Cr on Fe are different, as postulated previously from STM studies of the Cr growth on Fe whiskers [19] and of the Fe growth on the Cr single crystal [20], and from the CEMS studies of the Fe/Cr multilayers [7].

When non-equivalent interfaces were introduced to our interface model, the agreement between the experimental and simulated distributions of B_{hf} became reasonable and the contributions of different spectral components could be reproduced within $\pm$ 3%. The resulting concentration profile of Fe in the film of the nominal thickness 6 ML is shown in Fig. 5. The lower interface is relatively sharp and the Cr atoms are found in two layers only, whereas the upper interface is formed by at least three layers, in which the Cr concentration is considerable. Till now, such enhanced Fe–Cr intermixing was reported only at elevated preparation [21] or annealing [20] temperatures. The previous data concerned however a single crystalline substrate—the Fe whiskers [21] or the Cr single crystals [20]. The presently observed interfacial alloying at the room temperature is favored by the step-like structure of the Cr buffer layer. It is in the close agreement with the STM observation by Choi et al. [20] that steps or island edges work as the reaction sites for incorporation of the Fe adatoms into the Cr substrate.

4. Conclusion

The conversion electron Mössbauer spectroscopy at low temperatures is a unique tool for studying the local structure of buried interfaces in the ultra thin Fe (0 0 1) films sandwiched between Cr(0 0 1) layers. The data analysis for the 1–14 ML films, based on the correlation between the distribution of the hyperfine parameters and the film structure, revealed a discontinuity of the magnetic properties for the film consisting of the 6 Fe monolayers. This effect was interpreted in terms of a modification of the magnetic structure in the Cr layers. The ^{57}Fe probe layer method proved that Cr/Fe and Fe/Cr interfaces are non-equivalent. The lower interface showed up to be smoother than the upper one. The Fe concentration profile obtained from the CEMS analysis displayed a considerable interface Fe–Cr alloying for the films deposited at the room temperature.

Acknowledgements

This work was supported by the Polish State Committee for Scientific Research, Grants No. 7 T08C 002 16 and 2 P03B 142 17.

References

[1] Bland JAC, Heinrich B. Ultrathin magnetic structures. Berlin: Springer, 1994.
[2] Baibich MN, Broto JM, Fert A, Ngyuen Van Dau F, Petroff F, Etienne P, Creuzet G, Friederich A, Chazelas J. Phys Rev Lett 1988;61:2472.
[3] Schad R, Barnas P, Belien P, Verbanck G, Potter CD, Fischer H, Lefebvre S, Bessiere M, Moshchalkov VV, Bruynseraede Y. J Magn Magn Mater 1996;156:339.
[4] Fawcett E. Rev Mod Phys 1998;60:209.
[5] Sonntag P, Bodeker P, Schreyer A, Zabel H, Hamacher K, Kaiser H. J Magn Magn Mater 1998;183:5.
[6] Unguris J, Celotta RJ, Pierce DT. Phys Rev B 1992;69:1125.
[7] Shinjo T, Keune W. J Magn Magn Mater 1999;200:598.
[8] Korecki J, Kubik M, Spiridis N, Ślęzak T. Acta Phys Pol A 2000;97:129.
[9] Ibach H, Henzler M. Electron spectroscopy for surface analysis. Berlin: Springer, 1997.
[10] Spiridis N, Korecki J. unpublished.
[11] Landes J, Sauer Ch, Brand RA, Zinn W, Mantl S, Kajcsos Zs. J Magn Magn Mater 1990;86:71.
[12] Klinkhammer F, Sauer Ch, Tsymbal E, Handschuh S, Leng Q, Zinn W. J Magn Magn Mater 1996;161:49.
[13] Dubiel SM, Żukrowski J. J Magn Magn Mater 1981;23:214.
[14] Żukrowski J, Liu G, Fritzsche H, Gradmann U. J Magn Magn Mater 1995;145:57.
[15] Demuynck S, Meersschaut J, Dekoster J, Swinnen B, Moons R, Vantomme A, Cottenier S, Rots M. Phys Rev Lett 1998;81:2562.
[16] Fuchs P, Petrov VN, Totland K, Landolt M. Phys Rev B 1996;54:9304.
[17] Rancourt DG, Ping JY. Nucl Instr and Meth B 1991; 58:85.
[18] Kubik M, Karaś W, Korecki J. to be published.
[19] Davies A, Stroscio Joseph A, Pierce DT, Celottaa RJ. Phys Rev Lett 1996;76:4175.
[20] Choi YJ, Jeong IC, Park J-Y, Kahng S-J, Lee J, Kuk Y. Phys Rev B 1999;59:10918.
[21] Venus D, Heinrich B. Phys Rev B 1995;53:R1733.